Journal of Power Sources 209 (2012) 184–188

Contents lists available at SciVerse ScienceDirect

Journal of Power Sources

journal homepage: www.elsevier.com/locate/jpowsour

Short communication

Optimum lithium-ion conductivity in cubic $Li_{7-x}La_3Hf_{2-x}Ta_xO_{12}$

Asha Gupta[a], Ramaswamy Murugan[b], M. Parans Paranthaman[c], Zhonghe Bi[c], Craig A. Bridges[c], Masahiro Nakanishi[c,d], Alexei P. Sokolov[c], Kee Sung Han[c], E.W. Hagaman[c], Hui Xie[a], C. Buddie Mullins[a,e], John B. Goodenough[a,*]

[a] Materials Research Program and the Texas Materials Institute, ETC 9.184, University of Texas, Austin, TX 78712, USA
[b] Department of Physics, Pondicherry University, Puducherry 605 014, India
[c] Chemical Sciences Division, Oak Ridge National Laboratory, Oak Ridge, TN 37831, USA
[d] Department of Chemistry, University of Tennessee, Knoxville, TN 37996, USA
[e] Departments of Chemical Engineering and Chemistry and Biochemistry, University of Texas, Austin, TX 78712, USA

ARTICLE INFO

Article history:
Received 1 February 2012
Received in revised form 21 February 2012
Accepted 23 February 2012
Available online 3 March 2012

Keywords:
Li-ion battery
Solid electrolyte
Garnet
$Li_{7-x}La_3Hf_{2-x}Ta_xO_{12}$
Li NMR
Ionic conductivity

ABSTRACT

The nominal Li concentration giving a maximum room temperature Li-ion conductivity $\sigma_{Li} \simeq 3.45 \times 10^{-4}$ S cm^{-1} with an $E_a \simeq 0.438$ eV in the system $Li_{7-x}La_3Hf_{2-x}Ta_xO_{12}$ fired in an alumina crucible at 1130 °C for 48 h occurs in the narrow range of $x = 0.45 \pm 0.05$. The samples were prepared by solid-state reaction and characterized by XRD, SEM, electrochemical impedance spectroscopy and ^{7}Li MAS NMR measurements.

Published by Elsevier B.V.

1. Introduction

Commercial Li-ion batteries presently use a flammable, organic liquid-carbonate electrolyte having a LUMO at about 1.0 eV below the electrochemical potential μ_{Li} of a lithium anode [1]. The mismatch between the energy of the LUMO and μ_{Li} requires formation of a passivating solid-electrolyte interphase (SEI) layer, which results in dendrite formation and safety problems on repeated charging. This problem has motivated search for a solid oxide Li^+ electrolyte having a Li^+-ion conductivity $\sigma_{Li} > 10^{-3}$ S cm^{-1} [2] and the bottom of its conduction band above μ_{Li}. With a lithium anode, Li is not robbed from the cathode in the formation of the anode passivating layer. Furthermore, solid Li^+ electrolytes can minimize the safety problem associated with dendrite formation upon repeated plating of lithium on the anode by blocking Li dendrite from reaching the cathode. Oxides with the garnet framework, e.g. $Li_{7-x}La_3Zr_{2-x}Ta_xO_{12}$, fired in an alumina crucible promise to meet these requirements [3]. We report here an investigation of another system, $Li_{7-x}La_3Hf_{2-x}Ta_xO_{12}$ to explore the nominal Li occupancy that gives the maximum σ_{Li}. Hf(IV) is even less susceptible to reduction by lithium than is Zr(IV). The resultant compounds were structurally characterized by powder X-ray diffraction and solid-state ^{7}Li NMR. The latter also provides information on the dynamic behavior of lithium and is complemented by variable-temperature impedance spectroscopy measurements that provide an assessment of the bulk ionic mobility in these materials.

2. Experiment

Members of the $Li_{7-x}La_3Hf_{2-x}Ta_xO_{12}$ ($x = 0.1$–0.6) series were synthesized in alumina crucibles by conventional solid-state (ceramic) reaction of the starting materials taken in stoichiometric proportion. A small, undetermined amount of adventitious Al^{3+} in the garnet framework stabilizes the cubic structure to the high temperature needed for sintering pellets [4]. The precursor materials used was anhydrous LiOH (Alfa Aesar 99.5%, dried at 200 °C overnight; 10 wt.% excess was taken to compensate for the loss of lithium under annealing conditions), La_2O_3 (Alfa Aesar, treated at 950 °C overnight), HfO_2 (Alfa Aesar, 98%) and Ta_2O_5 (Alfa Aesar, 99.85%). The reactants were mixed with a mortar and pestle before reacting them at 950 °C for 12 h. The resultant product was reground and pressed into pellets. The pellets were transferred to an alumina crucible and covered with mother powder from all

* Corresponding author. Fax: +1 512 471 7681.
E-mail address: jgoodenough@mail.utexas.edu (J.B. Goodenough).

0378-7753/$ – see front matter. Published by Elsevier B.V.
doi:10.1016/j.jpowsour.2012.02.099

sides, followed by sintering at 1130 °C for 48 h to form single-phase material.

The products were characterized by powder X-ray diffraction (XRD) (Philips X'Pert Diffractometer, Cu Kα radiation) to monitor formation of the garnet phase. The structures were refined by the Rietveld method with the Fullprof-fp2k program [5,6]. For this purpose, XRD data were collected at a scan rate of 0.25° 2θ min^{-1} with 0.02° step size in the 2θ range between 10° and 90°.

The surface morphology of the sintered pellets was investigated in a scanning electron microscope Quanta FEG650. The relative densities of the sintered pellets were obtained at room temperature with the Archimedes' principle and deionized water as the immersion medium.

^{7}Li static and MAS NMR measurements were carried out at Oak Ridge National Laboratory on ground powders using a 9.4 T Bruker Avance NMR spectrometer. ^{7}Li MAS NMR spectra were acquired at Larmor frequencies of 155.3 MHz. Room temperature MAS measurements were made with a 4 mm MAS probe at spinning speeds of 15 kHz. ^{7}Li spectra were acquired with an echo sequence (90°-τ-180°) having a 90° pulse length of 2 μs. ^{7}Li chemical shifts are given with respect to 1 M LiCl ($\delta = 0$ ppm) using solid LiCl as secondary standard (−1.06 ppm).

Ionic conductivity of the pellets was measured using gold electrodes in the temperature range −50 to 100 °C in parallel-plate geometry. A Novocontrol Fourier response impedance analyzer was used in the frequency range from 10 to 10^{7} Hz and an Agilent E4991A RF-impedance analyzer was used in the frequency range 10^{6} to 3×10^{9} Hz. The same sample cell was used for both frequency ranges. A small piece of Pt mesh was sandwiched between the sample and probe electrodes in order to create good contact, and the temperature of the sample was controlled by a Novocontrol Quatro Cryosystem with flowing nitrogen gas.

3. Results and discussion

Powder XRD pattern for $Li_{7-x}La_3Hf_{2-x}Ta_xO_{12}$ ($x = 0.1$–0.6) series after their final heating stage are presented in Fig. 1. A small impurity peak is observed at 20.3° for $x = 0.2$; it is due to formation of the Li_2ZrO_3 phase (marked by * in Fig. 1). A few additional weak reflections were visible in some samples at ≤1% of the main peak intensity that could not be clearly identified, corresponding to a small impurity. Otherwise, all the XRD patterns are virtually identical and could be indexed to the cubic garnet framework in space group Ia-3d. Our samples do not show any additional diffraction lines due to tetragonal symmetry, as reported recently for $Li_7La_3M_2O_{12}$ (M = Zr, Sn) [7,8]. Murugan et al. [9] have stabilized the cubic polycrystalline phase of nominal composition $Li_7La_3Zr_2O_{12}$ by conventional solid-state reaction in an alumina crucible at high temperature (1200 °C).

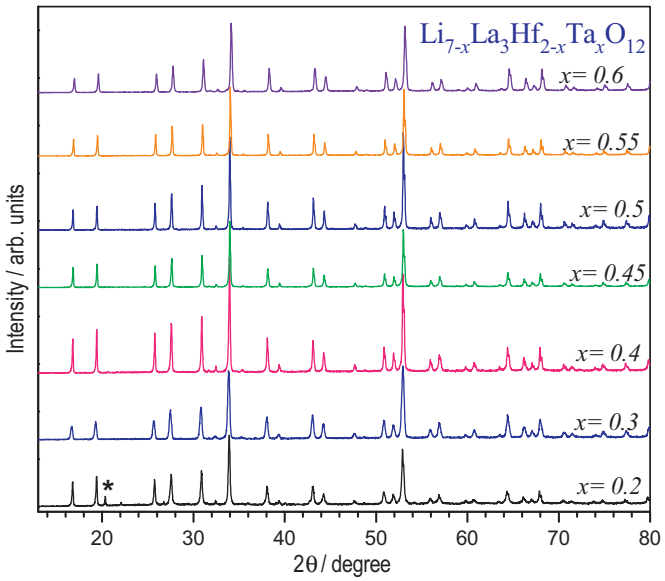

Fig. 1. Powder XRD pattern of $Li_{7-x}La_3Hf_{2-x}Ta_xO_{12}$ ($x = 0.2$–0.6) after sintering at 1130 °C for 48 h.

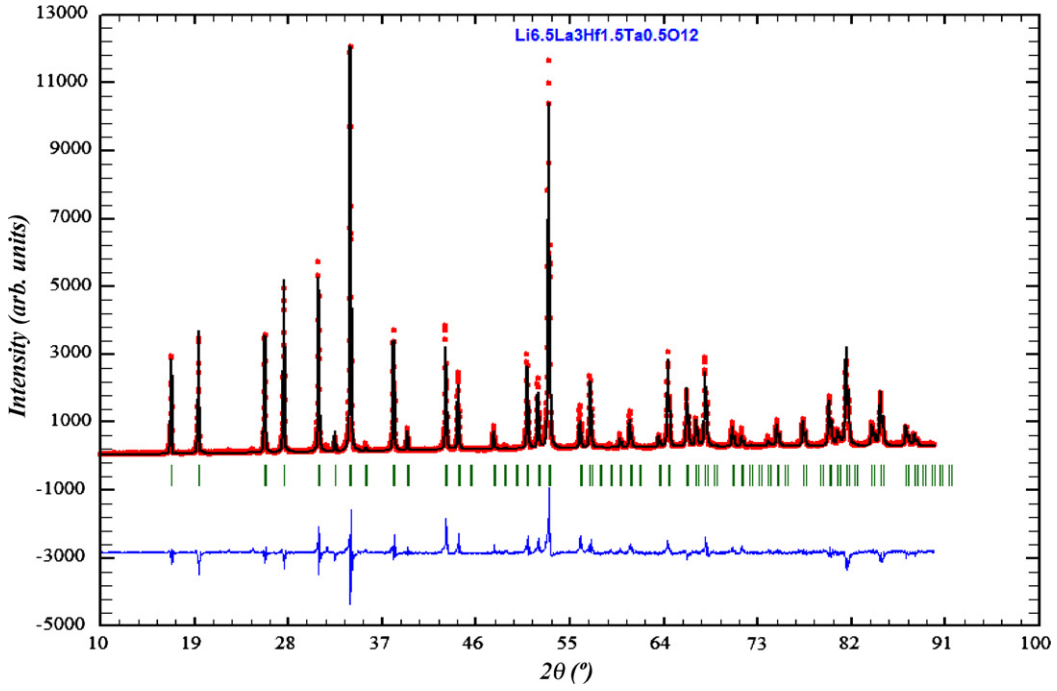

Fig. 2. Observed (red dots), calculated (black line) and difference XRD pattern (blue line) collected from $Li_{6.5}La_3Hf_{1.5}Ta_{0.5}O_{12}$ at room temperature. The lower green tick marks indicate allowed Bragg reflections from the garnet phase. (For interpretation of the references to color in this figure legend, the reader is referred to the web version of the article.)

Table 1
Structural parameters, activation energy, and total ionic conductivity for $Li_{7-x}La_3Hf_{2-x}Ta_xO_{12}$.

$Li_{7-x}La_3Hf_{2-x}Ta_xO_{12}$	Lattice parameter, a (Å)	R_f	R_{Bragg}	Relative density, %	Activation energy, E_a (eV)	Total conductivity ($S\,cm^{-1}$) at 22 °C
$x=0.2$	12.9439(7)	5.27	7.29	92.1		1.58×10^{-4}
$x=0.3$	12.9399(8)	7.94	9.63	92.4	0.448	1.83×10^{-4}
$x=0.4$	12.9362(4)	7.77	9.21	92.5	0.440	2.99×10^{-4}
$x=0.45$	12.9330(2)	5.61	8.11	93.2	0.438	3.45×10^{-4}
$x=0.5$	12.9298(2)	7.19	11.0	93.3	0.465	2.61×10^{-4}
$x=0.55$	12.9257(2)	5.14	7.07	90.3		2.21×10^{-4}
$x=0.6$	12.9275(3)	7.54	11.2	88	0.471	2.20×10^{-4}

Refinement of the XRD patterns was carried out by simultaneously varying parameters that include the overall structure factor, background parameters, unit cell, profile parameters, and isotropic thermal parameters; the Ta (V) ion was taken to be in Hf (IV) sites. The typical observed XRD patterns along with the calculated pattern are shown Fig. 2. The goodness of the profile refinements were determined from the R values, given in Table 1. A decrease in lattice parameter is observed with an increase in Ta substitution, which is consistent with the substitution of the smaller Ta (V) (ionic radius, $r=0.68$ Å in VI coordination) for the larger Hf (IV) ($r=0.97$ Å in VI coordination ion). Hence, our XRD results indicate that doping of the cubic garnet structure with Ta was successfully achieved in the composition range $x=0.2$–0.6.

The density of the pellets has a direct effect on the bulk conductivity. High density indicates the presence of relatively thin grain boundaries. For members of the series $Li_{7-x}La_3Hf_{2-x}Ta_xO_{12}$ ($x=0.1$–0.6), the highest relative densities were observed for Ta = 0.45 and 0.5 (see Table 1); it is, therefore, expected that the highest total lithium conductivity would be observed for these compositions.

The Nyquist plots at room temperature for the series are presented in Fig. 3a. The shapes of the impedance plots are similar to those previously reported for garnet-type materials, and the appearance of a low-frequency tail (high Z' values) indicates blocking of the mobile ions by the Au electrodes in these materials. The impedance spectra were fitted to an equivalent circuit, and

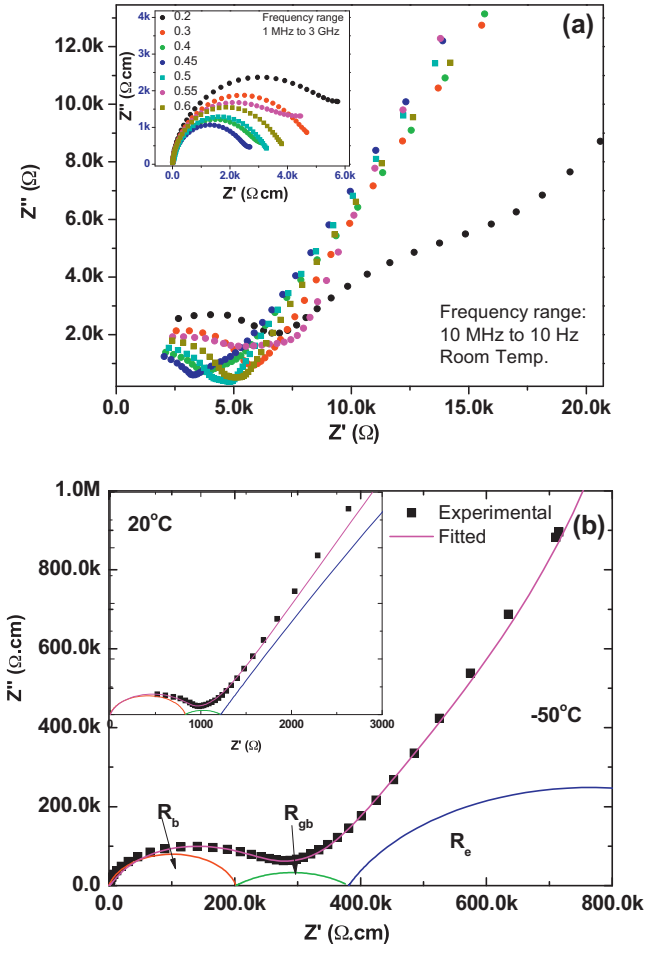

Fig. 3. (a) AC impedance of $Li_{7-x}La_3Hf_{2-x}Ta_xO_{12}$ ($x=0.2$–0.6) at room temperature from 10 MHz to 10 Hz. The inset shows the high frequency tail measured from 1 MHz to 3 GHz. (b) AC impedance spectra of $Li_{6.5}La_3Hf_{1.5}Ta_{0.5}O_{12}$ ($x=0.5$) at −50 and 100 °C with fitting data.

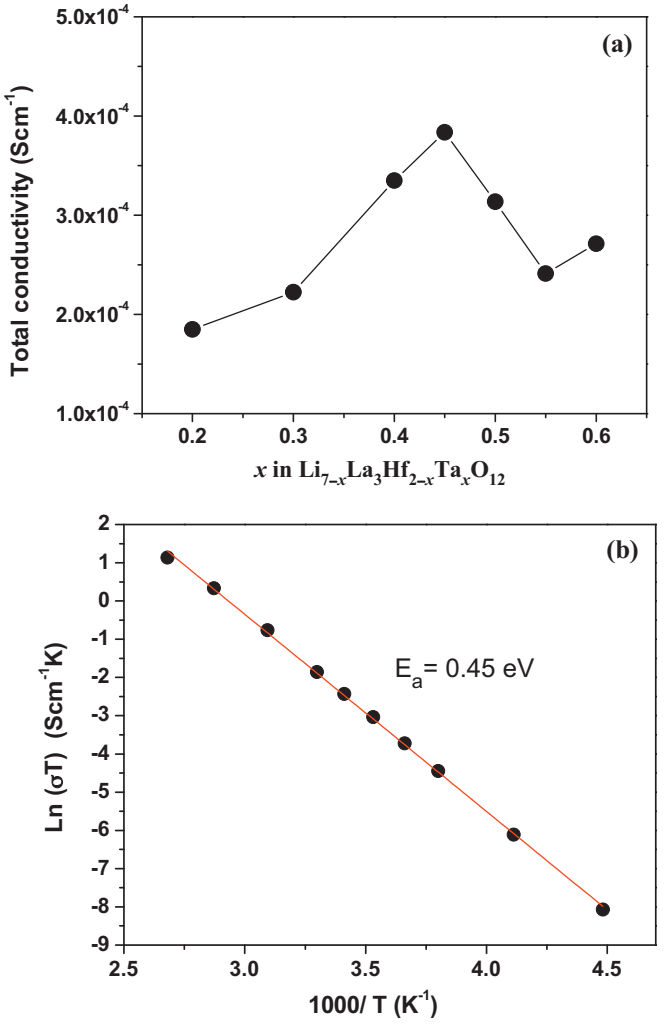

Fig. 4. (a) A plot of total conductivity at room temperature versus Ta concentration. (b) The Arrhenius plot for lithium ion conductivity of the $Li_{6.55}La_3Hf_{1.55}Ta_{0.45}O_{12}$ sample. The black circles represent the data and the red line is the fit to the data. (For interpretation of the references to color in this figure legend, the reader is referred to the web version of the article.)

resistance and capacitance values were extracted for the bulk, grain boundary and electrodes, separately. Fig. 3b shows an example for the $x = 0.5$ sample at −50 and 20 °C. The geometrical capacitance of the R_b was calculated to be $\sim 10^{-12}$ F cm^{-2}, where R_b has been assigned to represent the bulk resistance. For the intermediate-frequency arc R_{gb} and low-frequency R_e, the capacitance values are $\sim 10^{-10}$ F cm^{-2} and $\sim 10^{-8}$ F cm^{-2} respectively. With increasing temperature from −50 to 20 °C (Fig. 3b), the contribution of the grain-boundary resistance becomes smaller and the first intercept with the real axis at high frequency moves from ~3.1 kHz at −50 °C to 484 kHz at 20 °C, which reflects the enhanced Li ion mobility in the bulk at higher temperature. The bulk conductivities (σ_{Li}) of pellets of $Li_{7-x}La_3Hf_{2-x}Ta_xO_{12}$ ($x = 0.1$–0.6) observed at room temperature were attained by fitting the impedance spectra; they are tabulated in Table 1. A plot of the bulk conductivity versus molar Ta concentration, x, in nominal $Li_{7-x}La_3Hf_{2-x}Ta_xO_{12}$ is presented in Fig. 4a. The ionic conductivity is highest for the composition $x = 0.45$ and is of the same order as that previously reported for the nominal $Li_7La_3Zr_2O_{12}$ structure [7]. The temperature dependence of the bulk lithium-ion conductivity of $Li_{6.55}La_3Hf_{1.55}Ta_{0.45}O_{12}$ material prepared by solid state synthesis is shown in Fig. 4b; it can be expressed by the Arrhenius equation.

$$\sigma = \frac{A}{T} \exp\left(\frac{-E_a}{k_B T}\right)$$

where σ is the ionic conductivity, T the absolute temperature, A the pre-exponential constant, k_B the Boltzmann constant, and E_a the activation energy for the ionic conductivity. E_a was determined from the slope of the log (σT) versus $1/T$ plot. The calculated E_a in the temperature range of −50–100 °C for the different Ta concentrations is given in Table 1.

Previous studies of Li^+ transport in the garnet framework have suggested that the octahedral site (M = Hf, Ta) of the framework controls the relative Li^+ occupancies of the interstitial tetrahedral and octahedral sites [9–14]. Li self-diffusion in the garnet framework can be probed directly by diffusion-controlled ^{7}Li spin-lattice relaxation. ^{7}Li NMR spectra of $Li_{7-x}La_3Hf_{2-x}Ta_xO_{12}$ ($x = 0.2$–0.6) are presented in Fig. 5 as a function of the Ta substitution level, x. The static ^{7}Li NMR spectra display a central transition ($-1/2 \rightarrow 1/2$) resonance at 0.1 ppm, whose ^{7}Li resonance position is

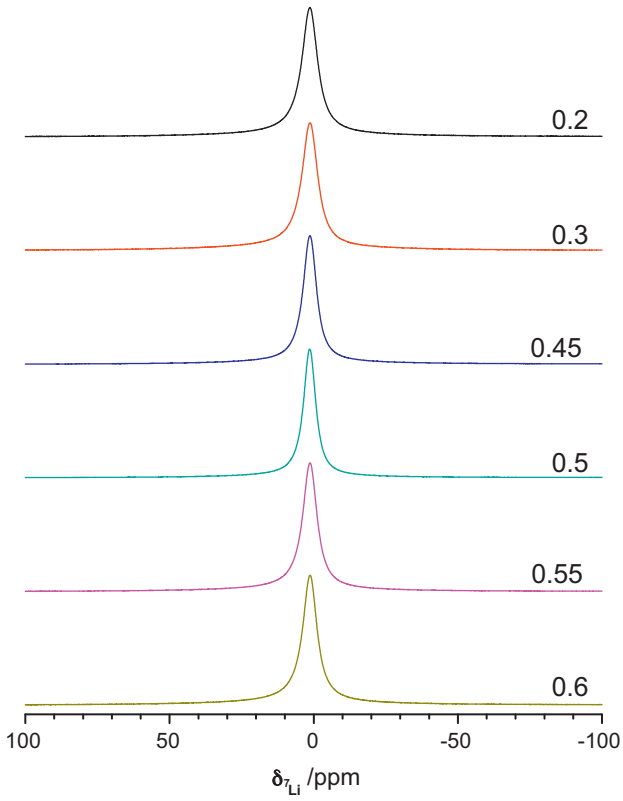

Fig. 5. Static ^{7}Li NMR spectra of $Li_{7-x}La_3Hf_{2-x}Ta_xO_{12}$ ($x = 0.2$–0.6). The spectra show the minimum line width at $x = 0.5$.

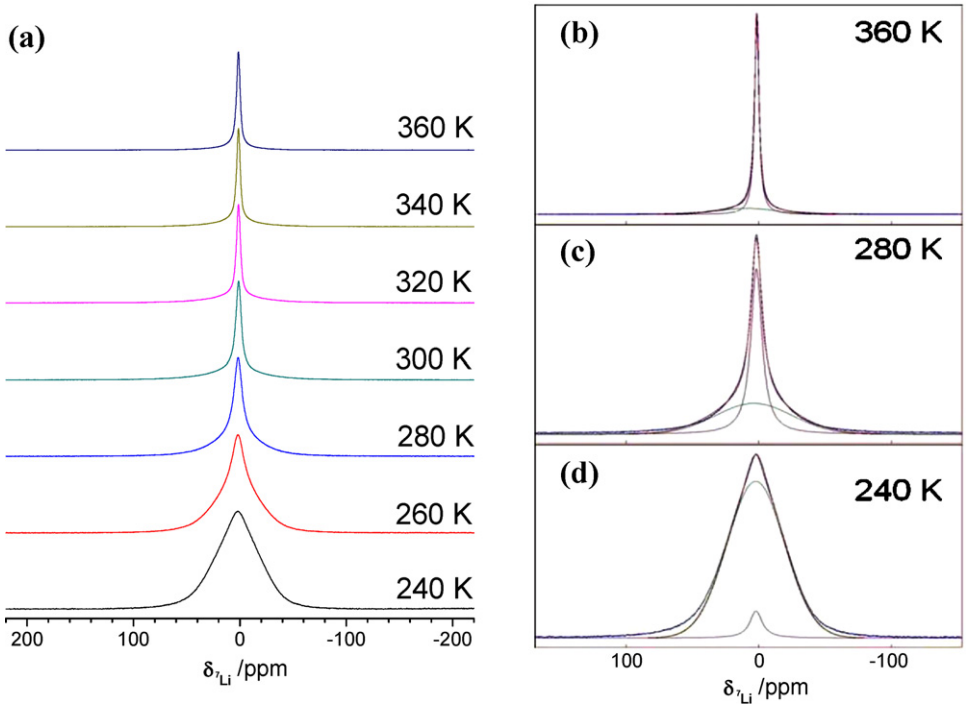

Fig. 6. (a) Static ^{7}Li NMR spectra of $Li_{6.5}La_3Hf_{1.5}Ta_{0.5}O_{12}$ as a function of temperature. (b) The line shape is fit as a sum of broad (Gaussian) and narrow (Lorentzian) component associated with fixed (slow) and mobile (fast) lithium ion domains.

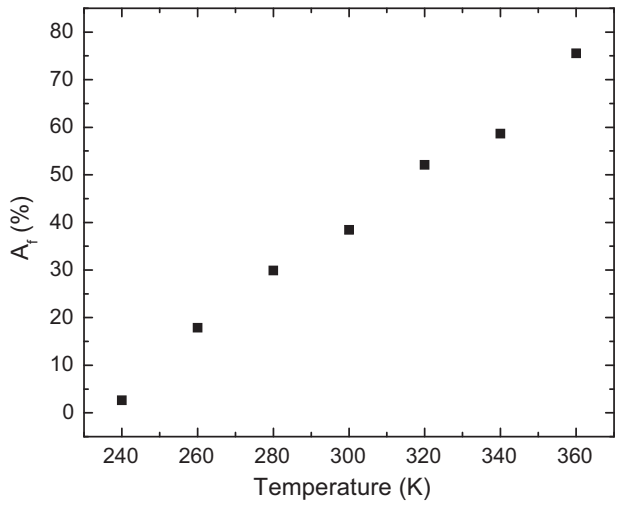

Fig. 7. Temperature dependence of the concentration of fast lithium ions, A_f, in static ^{7}Li NMR spectra of $Li_{6.5}La_3Hf_{1.5}Ta_{0.5}O_{12}$.

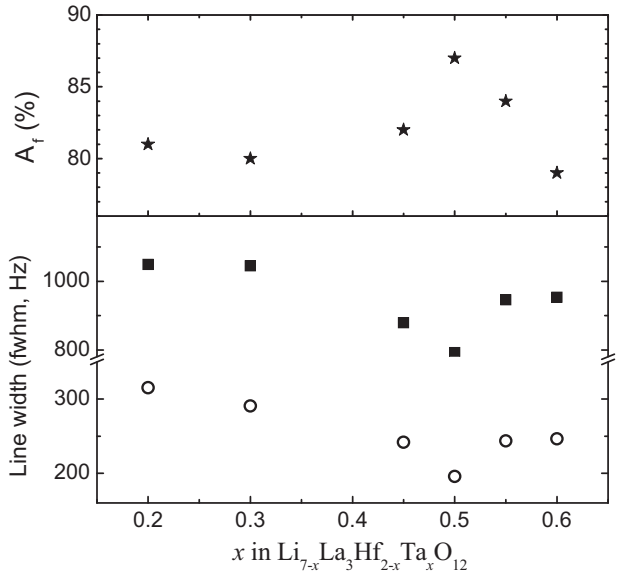

Fig. 8. Line width (FWHM) of ^{7}Li static (■) and MAS (○) NMR spectra of $Li_{7-x}La_3Hf_{2-x}Ta_xO_{12}$ as a function of x. The ^{7}Li MAS NMR FWHM are reduced a factor of ca. 4 relative to those of static spectra due to the absence of heterogeneous broadening. Both static and MAS spectra show the narrowest line width at $x = 0.5$. The fraction of highly mobile lithium ion, A_f(*) plotted separately, peaks at the same composition.

insensitive to the composition change of the solid electrolyte. The line width at half maximum height, FWHM, shows a minimum value at $x = 0.5$ that increases as x varies from this optimally narrow value. FWHM is a monitor on Li-ion mobility as a function of temperature in garnet materials [15,16]. The temperature dependence of the ^{7}Li resonance of $Li_{6.5}La_3Hf_{1.5}Ta_{0.5}O_{12}$ is shown in Fig. 6a. Here it is clear from the line shape that the resonance is a composite of a broad and a narrow component, which can be assigned to ^{7}Li populations with higher and lower ion mobilities. Fig. 6b–d shows representative deconvolutions of the composite line shape. The fractions of fast and slow Li ions in the sample can be determined by fitting the spectra as the sum of two components with Lorentzian (fast) and Gaussian (slow) line shapes. The fraction of the more mobile component, A_f, is plotted in Fig. 7. A_f increases linearly with temperature over the temperature range investigated.

The FWHM of the static ^{7}Li spectra of Fig. 5 are plotted in Fig. 8, along with the FWHM determined from the MAS spectra (not shown). The MAS line widths are reduced a factor of ca. 4 from the static spectra, but otherwise they show the same response as a function of Ta substitution level. A_f is compared with the line widths for the composition series. The minimum in FWHM and maximum in A_f occur concurrently and show that the greatest lithium ion mobility occurs for the composition with $x = 0.5$. Based on FWHM, $x = 0.5$ shows the narrowest line width, indicating that bulk Li mobility is highest for this concentration of Ta. This is in contrast to the impedance data, which showed the highest ionic conductivity for Ta = 0.45. However, the NMR data were taken on powder samples and represent the bulk σ_{Li} whereas the impedance data reflects the total σ_{Li} including both the bulk and grain-boundary contributions.

4. Conclusion

The effect on the Li^+ conductivity of pentavalent Ta substitution for tetravalent Hf in nominal $Li_{7-x}La_3Hf_{2-x}Ta_xO_{12}$ has revealed an optimum Ta concentration per formula unit of $x = 0.45$ for a total Li^+ conductivity of 3.45×10^{-4} S cm^{-1} at room temperature (22 °C) whereas NMR data gave an optimum $x = 0.5$ for the bulk conductivity. The maximum Li conductivity in this system is smaller than that in nominal $Li_{7-x}La_3Zr_{2-x}Ta_xO_{12}$ but it occurs in the same narrow range of x where the neutron data [4] indicate that short-range order of the Li^+ ions in the interstitial space is initiated. We suggest that the two types of Li^+ mobility observed by NMR reflect a progressive transition from short-range order to disorder with increasing temperature near room temperature.

Acknowledgements

The authors at the University of Texas at Austin gratefully acknowledge The Robert A Welch Foundation of Houston, Texas [grant numbers F-1066 for JBG and F-1436 for CBM] and the Department of Energy Office of Basic Energy Science grant DE SC00005397. MPP and CAB were supported by the US Department of Energy, Basic Energy Sciences, Materials Science and Engineering Division. APS acknowledges the financial support from the LDRD Program of ORNL (LOIS 5608), managed by UT-Battelle, LLC for US Department of Energy. ZB acknowledge the support of the ORISE postdoctoral fellowship. EWH and KSH were supported by the Division of Chemical Sciences, Geosciences, and Biosciences, Office of Basic Energy Sciences, US Department of Energy.

References

[1] J.B. Goodenough, Y. Kim, Chem. Mater. 22 (2010) 587.
[2] T. Lapp, S. Skaarup, A. Hooper, Solid State Ionics 11 (1983) 97–103.
[3] L. Yutao, C.-A. Wang, H. Xie, M. Xu, J. Han, J. Cheng, J.B. Goodenough, Unpublished work.
[4] H. Xie, J.A. Alonso, Y. Li, M.T. Fernandez-Díz, J.B Goodenough, Chem. Mater. 23 (2011) 3587.
[5] T. Roisnel, J. Rodriguez-Carvajal, Epdic7, Eur. Powder Diffract. 378-3 (2001) (Pts 1 and 2) 118.
[6] J. Rodriguez-Carvajal, J. Phys. 192B (1993) 55.
[7] J. Percival, E. Kendrick, R. Smith, P. Slater, Dalton Trans. 35 (2009) 5177–5181.
[8] J. Awaka, N. Kijima, H. Hayakawa, J.J. Akimoto, Solid State Chem. 182 (2009) 2046–2052.
[9] R. Murugan, V. Thangadurai, W. Weppner, Angew. Chem. Int. Ed. 46 (2007) 7778–7781.
[10] V. Thangadurai, H. Kaack, W. Weppner, J. Am. Ceram. Soc. 86 (2003) 437–440.
[11] J. Percival, E. Kendrick, P. Slater, Solid State Ionics 179 (2008) 1666–1669.
[12] R. Murugan, V. Thangadurai, W. Weppner, Appl. Phys. A: Mater. Sci. Process. 91 (2008) 615–620.
[13] E.J. Cussen, Chem. Commun. (2006) 412–413.
[14] O'Callaghan, M. Powell, A. Titman, J. Chen, G. Cussen E, J. Chem. Mater. 20 (2008) 2360–2369.
[15] L.V. Wullen, T. Echelmeyer, H.W. Meyer, D. Wilmer, Phys. Chem. Chem. Phys. 9 (2007) 3298–3303.
[16] B. Koch, M. Vogel, Solid State Nucl. Magn. Reson. 34 (2008) 37–43.